Title:	Influence of flanges on the shear-carrying capacity of reinforced concrete beams without web reinforcement
Authors:	Ribas González C. R., Fernández Ruiz M.
Published in:	Structural concrete
DOI	10.1002/suco.201600172
Volume: Pages:	18 pp. 720-732
Year of publication:	2017
Type of publication:	Peer reviewed journal article

Please quote as:	Ribas González C. R., Fernández Ruiz M., *Influence of flanges on the shear-carrying capacity of reinforced concrete beams without web reinforcement*, Structural concrete, 18, 2017, pp. 720-732.

Received: 6 October 2016 | Revised: 29 January 2017 | Accepted: 8 March 2017

DOI: 10.1002/suco.201600172

WILEY fib CEB-FIP

TECHNICAL PAPER

Influence of flanges on the shear-carrying capacity of reinforced concrete beams without web reinforcement

Carlos Rodrigo Ribas González[1] | Miguel Fernández Ruiz[2]

[1]Department of Physics, Universitat de les Illes Balears, Palma, Spain

[2]IBETON, École Polytechnique Fédérale de Lausanne, Lausanne, Switzerland

Correspondence
Carlos Rodrigo Ribas González, Department of Physics, Universitat de les Illes Balears, Carretera de Valldemossa km 7.5, Edifici Mateu Orfila, Palma de Mallorca, Islas Baleares 07122, Spain
Email: carlos.ribas@uib.es

Funding information
Swiss Confederation, Grant/Award number: AGB-2006-015; Spanish Ministry of Economics and the European Funds for Regional Development (Horvital), Grant/Award number: BIA2015-64672-C4-3-R.

T-beams are acknowledged as economic and efficient structural members widely used for floor slab construction systems. In many cases, according to practice in some countries, the beams do not present transverse reinforcement, and their shear strength is governing for dimensioning the width of the web. Although experimental investigations have shown that the presence of the compression flange enhances the shear capacity with respect to equivalent rectangular cross sections, most current design codes neglect this phenomenon, which leads to the overdesign of these members. In this paper, the role of the compression flange of slender T-beams with concentrated loads is investigated with reference to its influence on the shape of the critical shear crack and to the associated shear transfer actions (STA) of the beam. The flanges are considered elements that allow the smearing of applied loads over a certain length of the web. This consideration, in combination with the mechanical model of the Critical Shear Crack Theory (CSCT), allows a consistent treatment of the phenomenon and leads to simple design expressions accounting for the role of flanges. The results of the proposed model are compared together with design codes (Model Code 2010, Eurocode 2, and ACI 318-11) and other shear design approaches to a database of 239 beams on T-shaped members. The comparison shows that the role of flanges is finely accounted with the proposal based on the CSCT, leading to consistent agreement and to strength predictions that are more suitable for design purposes than the other investigated design models.

KEYWORDS
Critical Shear Crack Theory, flange–web interaction, shear strength, T-beams

1 | INTRODUCTION

Concrete T-beams without shear reinforcement have been widely used in order to build concrete ribbed slabs or beam-and-block floors[1–4] and are still used today as an economic and efficient construction system in many countries.[3] The use of this cross section without web reinforcement is normally related to structural floors, in which rows of T-beams are arranged at a given spacing (Figure 1a). The main purpose of this system is to remove concrete in the tension zone of the section, thus reducing the self-weight of the structure. Other structural floors are also equivalent to the structural behavior of T-beams as waffle or filler slabs (also called two-way ribbed slabs, Figure 1b). It can be noted that torsional effects are not governing for these members as torsion is taken by differential bending when two or more ribs are available (Figure 1a,b) instead of uniform torsion by each web.

The beneficial effects of the compression flange of a T-beam on the shear strength of members without transverse reinforcement is well acknowledged since early concrete research[1] and has particularly been investigated since the 1970s.[5,6] On that basis, several authors have published different approaches to assess the increase of shear strength due to the compression flange in a T-beam with simple

Discussion on this paper must be submitted within two months of the print publication. The discussion will then be published in print, along with the authors' closure, if any, approximately nine months after the print publication.

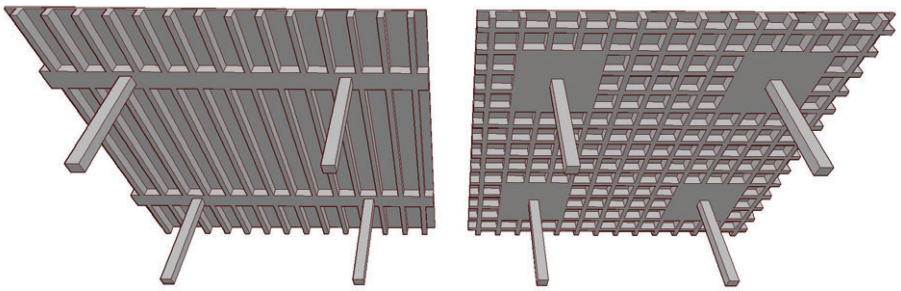

FIGURE 1 Concrete structural floors made of rows of T-beams without transverse reinforcement: (a) one-way ribbed slab and (b) two-way ribbed slabs.

design equations.[5–13] Most of these approaches deal with a shear-effective area, assuming that the area of the flange effective for increasing the shear strength is only uncracked and closer to the web. Figure 2 summarizes some relevant approaches of the shear-effective area of the compression chord in T-beams.[5–13] In most cases, the shear strength of the element is the result of multiplying this shear-effective area by an average nominal shear stress.

However, most of the current codes do not take into account the beneficial effect on the shear strength due to the flange in a T-beam, even though its beneficial role is in some cases explicitly acknowledged.[14]

2 | SHEAR TRANSFER ACTIONS IN REINFORCED CONCRETE MEMBERS AND PECULIARITIES OF T-SHAPED MEMBERS

2.1 | Shear transfer actions in T-beams

Shear transfer actions (STA) in beams without shear reinforcement and a rectangular cross section have been summarized recently by Fernández Ruiz et al.[15] These actions are normally classified into beam STA (Figure 3a, where the internal level arm remains constant) and the arching action (Figure 3f, where the lever arm varies). The three beams' STAs are normally named as cantilever action (Figure 3b), aggregate interlock (Figure 3c), doweling action (Figure 3d), and residual tensile strength of the concrete (Figure 3e).

As discussed in References 15 and 16, the activation of the various STA depends a great deal on the critical shear crack pattern and its associated kinematics. With respect to T-beams without transverse reinforcement, the critical shear crack pattern observed is slightly different to the one observed at a rectangular section beam. Figure 4 shows, for instance, two representative crack patterns of T-beams without transverse reinforcement, reported in References 17 and 18. Both specimens failed in shear but with a different shape of the critical shear crack. The former (Figure 4a) developed a diagonal shear crack that continued as a delamination crack at the flange interface and provoked a bending mechanism in the flange. In the latter (Figure 4b), the diagonal shear crack at the web continued on the contrary as an inclined crack in the flange and also in the second one. For both cases, a vertical crack can be observed

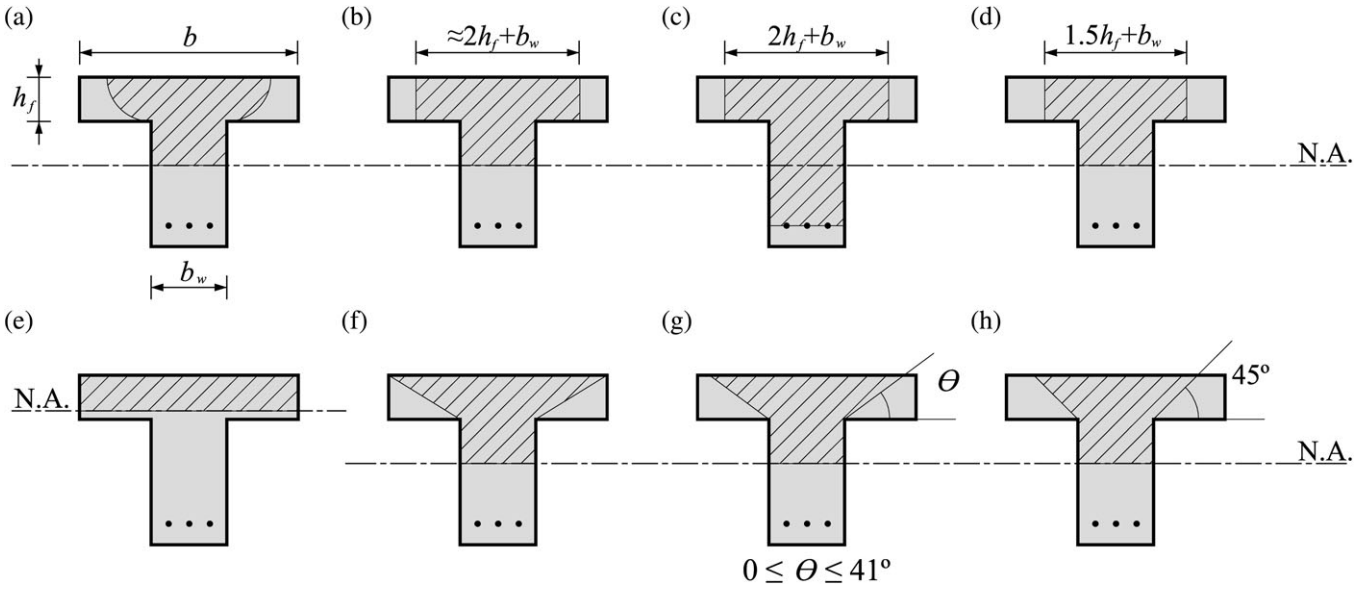

FIGURE 2 Different approaches to shear-effective area of the compression chord: (a) Leonhardt,[7] (b) Placas et al[5] and Cladera et al,[8] (c) Zsutty,[6] (d) Moayer and Regan,[9] (e) Swamy and Qureshi,[10] (f) Zararis et al,[11] (g) Tureyen et al,[12] and (h) Ribas et al.[13]

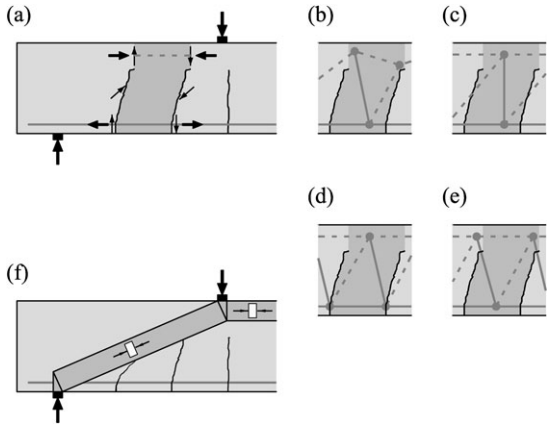

FIGURE 3 Shear transfer actions for beams with a rectangular cross section: (a) beam actions, (b) cantilever action, (c) aggregate interlock, (d) dowel action, (e) residual tensile strength of concrete, and (f) arching action.

starting from its upper side, appearing approximately at the location where the diagonal shear crack interrupts the flange, indicating bending of the compression flange. While the flange of Figure 4a clearly rotated, the flange of the beam presented in Figure 4b exhibited a lower level of rotation. These two patterns have been consistently observed in most of the T-beams without shear reinforcement reported in the literature.[9,10,18–21]

With respect to the bending of the flange, Figure 5 shows the measurements of two gauges on the flange and the crack evolution of one specimen tested by Ribas and Cladera.[4] It can be observed that prior to shear cracking (Figure 5c), both top and bottom gauges of the flange measured compression strains. As the load increased, the crack developed in an inclined manner (Figure 5d). It can be noted that the top gauge measured a reduction of the compression strains (Figure 5a), and eventually, tensile strains were measured near failure (Figure 5e). This agrees with the development of a flexural crack observed in Figure 4.

The STA that get involved in a T-beam are essentially the ones shown in Figure 3. Some differences, however, exist that can be explained through the analysis of the critical shear crack pattern in relation with the STA.[4,11,18,22,23] For instance, Figure 6a,b shows the critical shear crack pattern in its initial state, which starts from a bending crack and extends to approximately the neutral axis of the section. This behavior is similar for both types of beams, with rectangular cross section (Figure 6a) and T-beams (Figure 6b). As the load increases, a second branch of the critical crack develops above the neutral axis. This branch becomes flatter due to a failure of concrete tension tie in Figure 6a.[16] This phenomenon can also be explained by a combination of stresses as described, for instance, by Park et al.[24] This behavior occurs similarly for both beams, with rectangular section (Figure 6c) and T-beams, until the crack reaches the soffit of the flange (Figure 6d). In fact, for T-beams with large flanges, this crack develops horizontally (at the interface of the flange) as this corresponds to the weakest region of the tension tie (Figure 6d). Following the formation of the delamination crack, the concrete flange remains uncracked. This allows for the development of the pure arching action (Figure 3f) or even of the strut-and-tie model, with the elbow-shaped strut described by Muttoni and Schwartz[25] shown in Figure 6f. This latter model allows deviating the inclined concrete strut by activating tensile forces in the concrete (or in the longitudinal reinforcement in the flange if present) and is consistent with measurements of the strains on the upper face of the T-beams, tested by Swamy et al[17] and Ribas and Cladera[4] as previously discussed (Figure 5).

Failure of T-beam and the collapse of this STA occur simultaneously. The collapse of the latter can be caused by failure of the concrete of the flange in tension (Figure 6f).[10] Some authors, that is, Zararis et al,[11,26] also relate the failure to a strut-and-tie model similar to the one shown in Figure 6g, where dowel action is required. These two strut-and-tie models can explain the critical shear crack patterns reported by

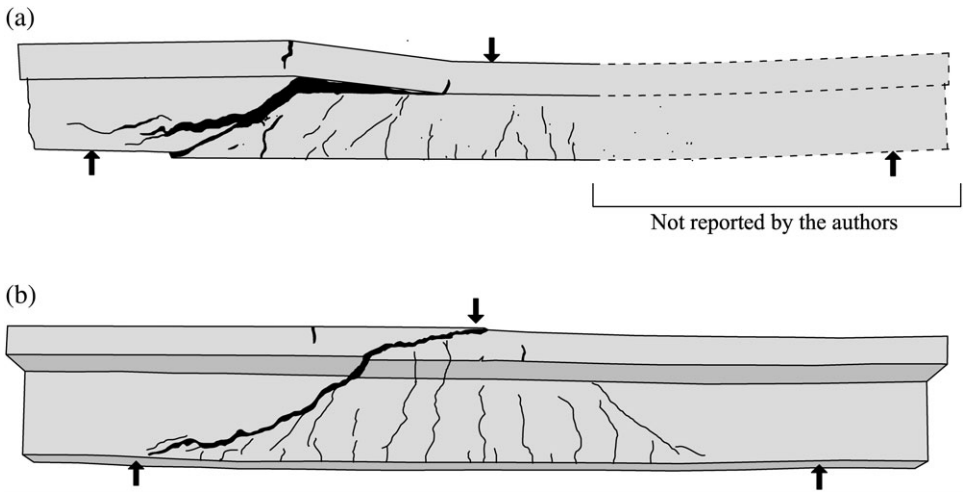

FIGURE 4 Crack patterns of T-beams without transverse reinforcement: (a) with delamination crack (adapted from Reference 17) and (b) with diagonal crack at the flange (adapted from Reference 18).

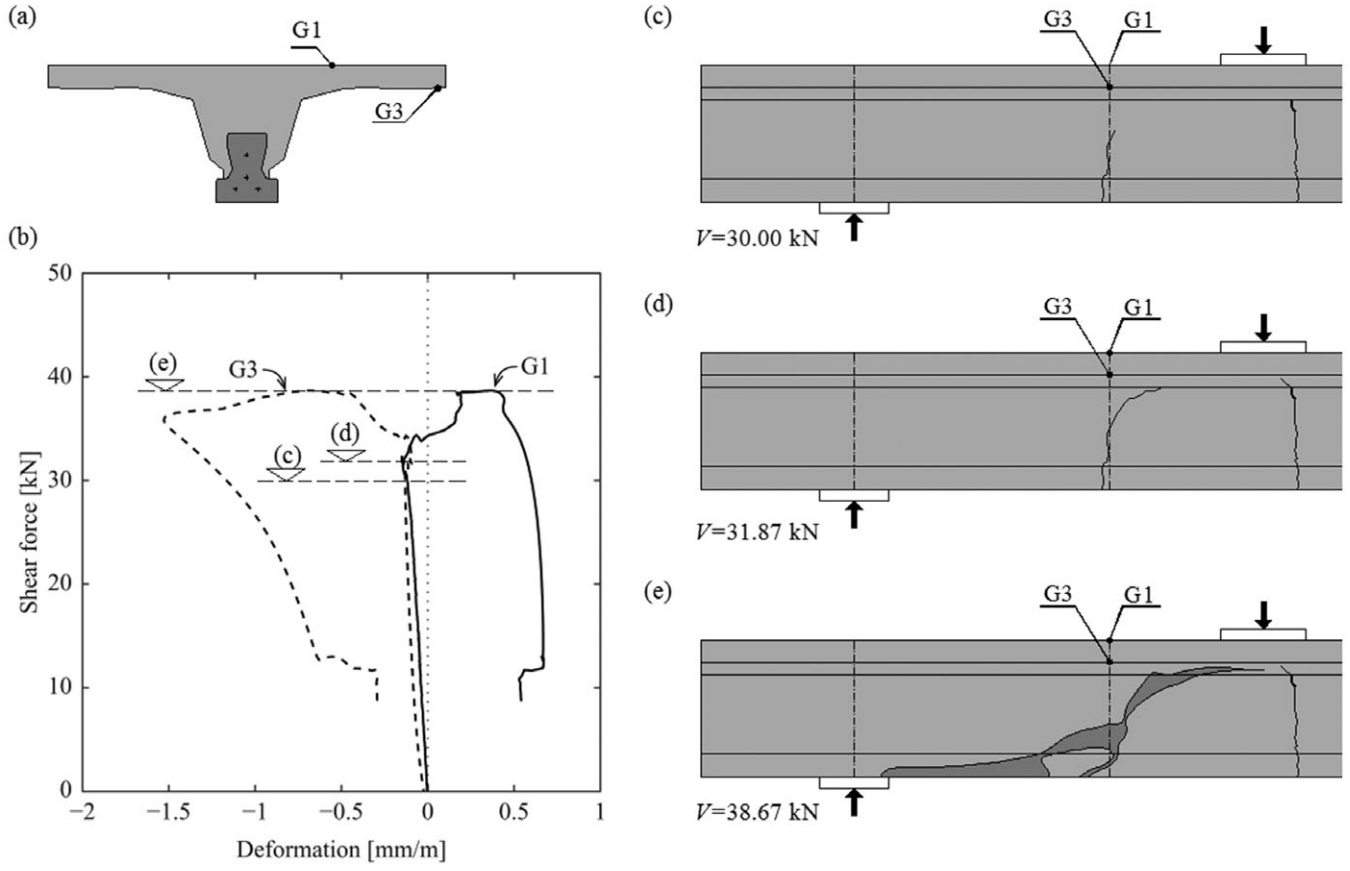

FIGURE 5 Strain measurements of a flange during a test:[4] (a) specimen instrumentation at the cross section, (b) gauges measurements, (c) bending-induced cracking, (d) crack rotation, and (e) cracking pattern at maximum load.

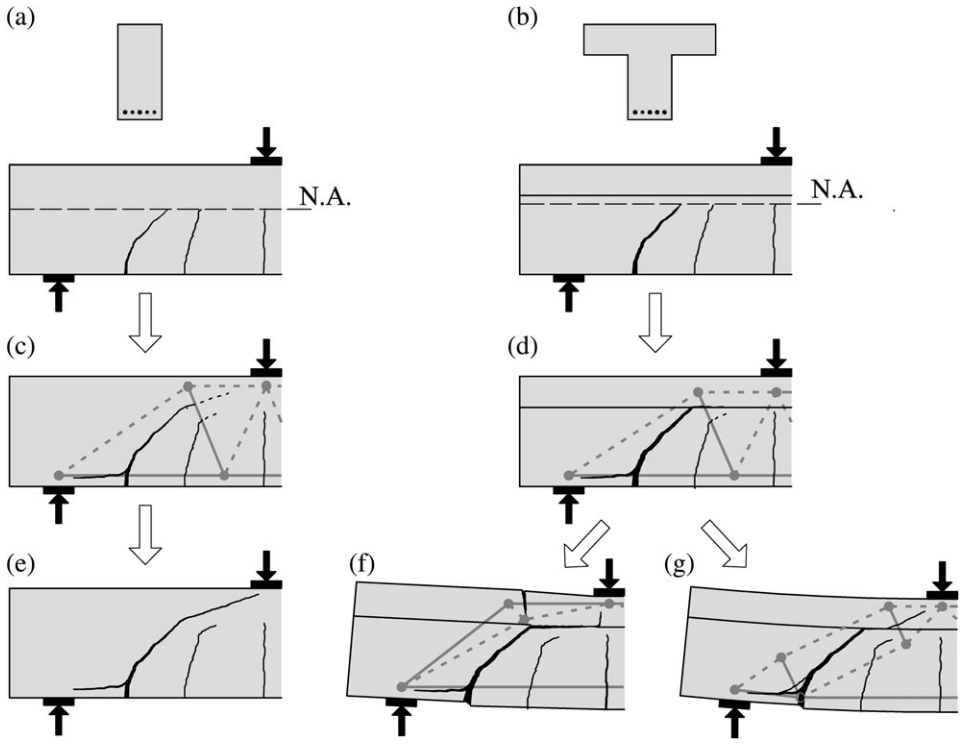

FIGURE 6 Critical shear crack pattern comparison between rectangular cross-section beams and a T-Beam: (a, b) flexural cracking, (c, d) development of inclined cracks, and (e–g) crack pattern at failure.

different authors,[9,17–20,23] shown in Figure 4a,b. A similar classification was made by Regan[22] taking into account the progress of the critical shear crack shown in Figure 6f,g.

It is also interesting to note that the strut-and-tie models showed in Figure 6f,g neglect the aggregate interlock in the inclined branch of the critical shear crack in the web. This fact is consistent with the experimental measurements of the critical crack width reported before shear failure: by Kotsovos et al for T-beams with a very high amount of longitudinal reinforcement,[23] and by Ribas and Cladera for elements with a section similar to a T (Figure 5a) and very low amount of longitudinal reinforcement (concentrated in a prestressed and precast joist)[4], where high crack openings were measured in both researchs.

2.2 | Influence of the shear slenderness on T-beams

With respect to the influence of shear slenderness on rectangular concrete members, two different responses have traditionally been acknowledged:[27] beams with shear span to depth ratio a/d lower than approximately 2.5 are capable of carrying partially the load by direct strut (arching action) as illustrated in Figure 3f (where a is the shear spam, and d is the effective depth). For rectangular beams with higher shear span to depth ratio, arching action is no longer governing, and beam STA (Figure 3a) control the shear strength.[15] This change of the governing model can be observed, for instance, in the results of a test campaign carried out by Swamy et al[17] and illustrated in Figure 7, where an abrupt change in the slope of the curve occurs at a value $a/d \approx 2.5$.

With respect to T-beams, this change in the governing STA is also observed. However, in this case, the crack pattern (with the delamination branch Figure 6f) allows arching action to develop for more slender members than those with a rectangular cross section.

Therefore, as it can be seen experimentally in Figure 7, the ratio a/d related to the change of the governing model in T-beams is higher (closer to 4) than for an equivalent rectangular cross-section beam. This implies that the bottom of Kani's valley is shifted with respect to beams with a rectangular section, from $a/d \approx 2.5$ to $a/d \approx 4$.[28] A physical justification for this experimental observation will be discussed later in this paper.

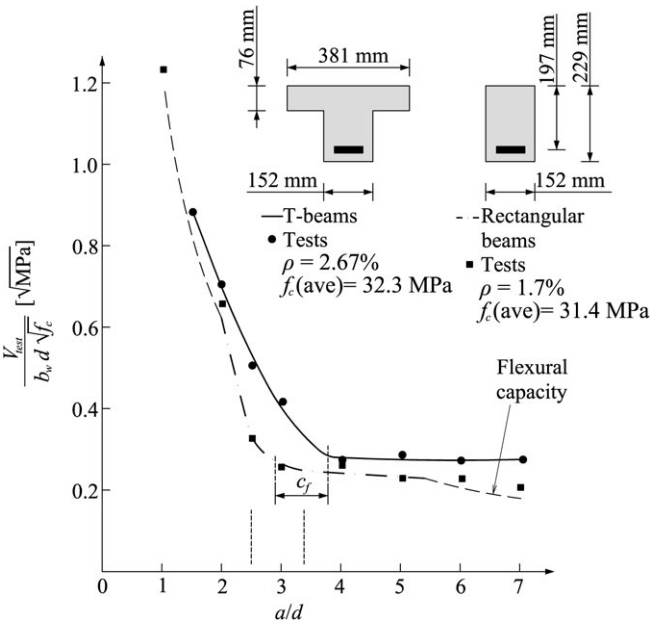

FIGURE 7 Swamy et al's test results for rectangular cross-section beams and for T-beams (adapted from Reference 17).

3 | SHEAR DESIGN OF T-BEAMS BASED ON THE CRITICAL SHEAR CRACK THEORY

As a result of what has been illustrated in Figures 6 and 7, the ratio h_f/d, where h_f is the depth of the flange, is essential to evaluate the shear strength of a T-beam. In the following sections, this will be investigated by using the mechanical model of the Critical Shear Crack Theory (CSCT).[15]

3.1 | Brief description of the CSCT

The CSCT is a rational approach to assess the shear strength of the slender concrete members without shear reinforcement.[15,16] The CSCT claims that the plasticity-based solutions with an inclined compression strut-carrying shear (Figure 3f) overestimate the shear strength when a critical shear crack develops through the theoretical strut. The CSCT takes into account the different STA presented in Figure 3 by assuming different contributions for each based on the shape of the critical shear crack and its associated kinematics. It is shown by means of analytical integration of the stresses that the shear strength at failure depends on the opening, roughness, and fracture energy properties of the critical shear crack.[15]

For rectangular-reinforced concrete beams without shear reinforcement, the width of the critical shear crack w is estimated proportionally to a reference longitudinal strain ε (see Figure 8a,b) times the effective depth of the member d.[16]

$$w \propto \varepsilon \cdot d \tag{1}$$

This relation was used to derive a failure criterion according to the following expression[15] see Figure 8c:

$$V_R = \frac{bd\sqrt{f_c}}{3} \frac{1}{1 + 120\frac{\varepsilon \cdot d}{d_{g0} + d_g}} \text{ [MPa, mm]} \tag{2}$$

where f_c is the concrete compressive strength, d_{g0} is a reference size of (16 mm), and d_g is the maximum aggregate size (in mm). The principal aspects of the CSCT failure criterion and of the analytical integration of the stresses developed at the critical shear crack have been summarized elsewhere.[15] The theory has been shown to account for the different

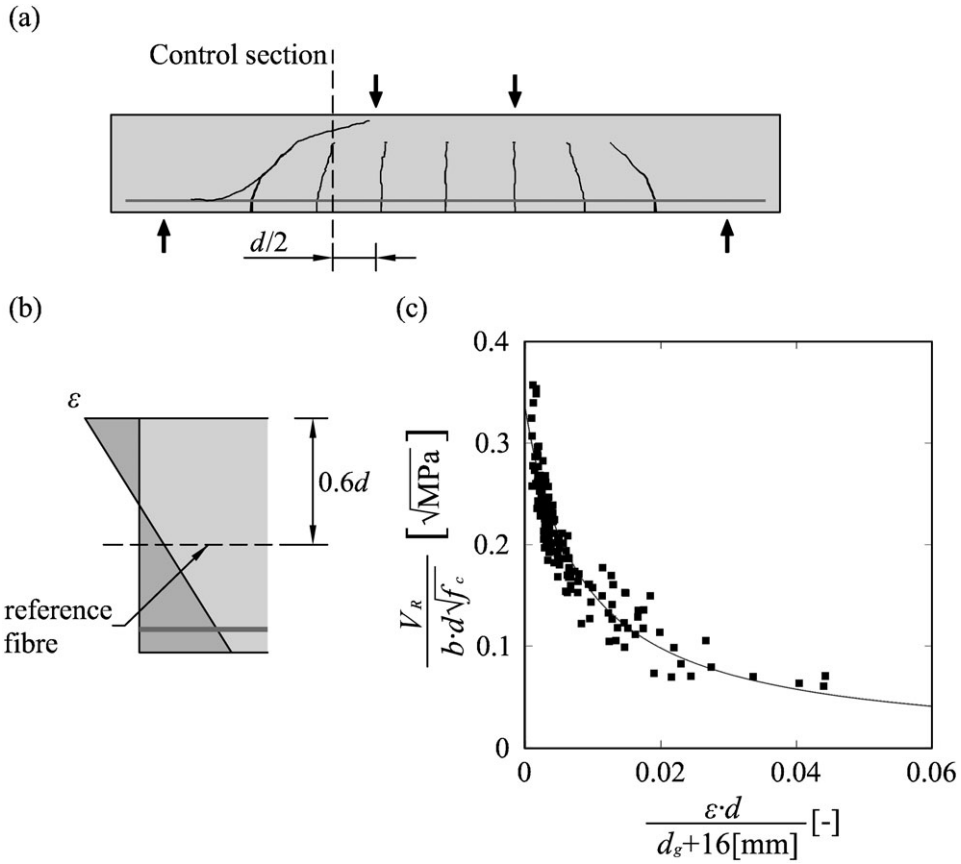

FIGURE 8 Failure criterion of the Critical Shear Crack Theory: (a, b) location of the control section and reference fiber and (c) failure criterion (Equation 2).

potential STA providing consistent treatment of strain and size effects. It has also been demonstrated[15] to be consistent with the size effect law,[29] providing a smooth transition between limit analysis and linear elastic fracture mechanics.

3.2 | Extension of the CSCT to T-beams

In order to evaluate the interaction between the web and the flange of a T-beam without transverse reinforcement subjected to point loading, an approach similar to the one presented by Rupf et al[30] for T-beams with transverse reinforcement will be followed (similar derivations apply to other loading cases). However, the approach originally proposed by Rupf et al[30] refers to beams with transverse reinforcement and thus, its basic assumptions have to be generalized to this case (members without stirrups). In the following, the T-beam is considered composed by two different elements as shown in Figure 9a,b. The first is the web of the beam, and the second element is the flange outside the web.

The compression flange is considered a beam where the deflections δ are governed by bending, neglecting the deflection produced by shear forces and assuming a constant stiffness EI_f along ξ (where E is the modulus of elasticity of concrete, I_f is the inertia of the outer part of the compression flange—referred as the flange hereafter—and ξ is the longitudinal axis as they are defined in Figure 9b,c). Therefore, the relation between the load applied to the flange and the deflection δ can be expressed as:

$$q_f = EI_f \cdot \frac{\partial^4 \delta}{\partial \xi^4} \tag{3}$$

where q_f is the distributed force applied by the web to the flange (Figure 9c,d).

However, the web will be considered a beam where deflections will be governed by both bending and shear. A constant shear and bending stiffness of the web will be assumed as GA_w and EI_w, respectively, where G is the concrete shear modulus, and A_w and I_w are the inertia and the area of the web as it is defined in Figure 9c, respectively. Consequently, the deflection δ of the web can be expressed as:

$$q_w = GA_w \cdot \frac{\partial^2 \delta}{\partial \xi^2} + EI_w \cdot \frac{\partial^4 \delta}{\partial \xi^4} \tag{4}$$

where q_w is the distributed force applied by the flange to the web (Figure 9d).

According to Rupf et al,[30] in the region of the beam cracked in shear where load transfer occurs between the flange and the web, the stiffness of the web is mostly governed by its shear deformation (the validity of this assumption[30] was based both on test measurements on seven

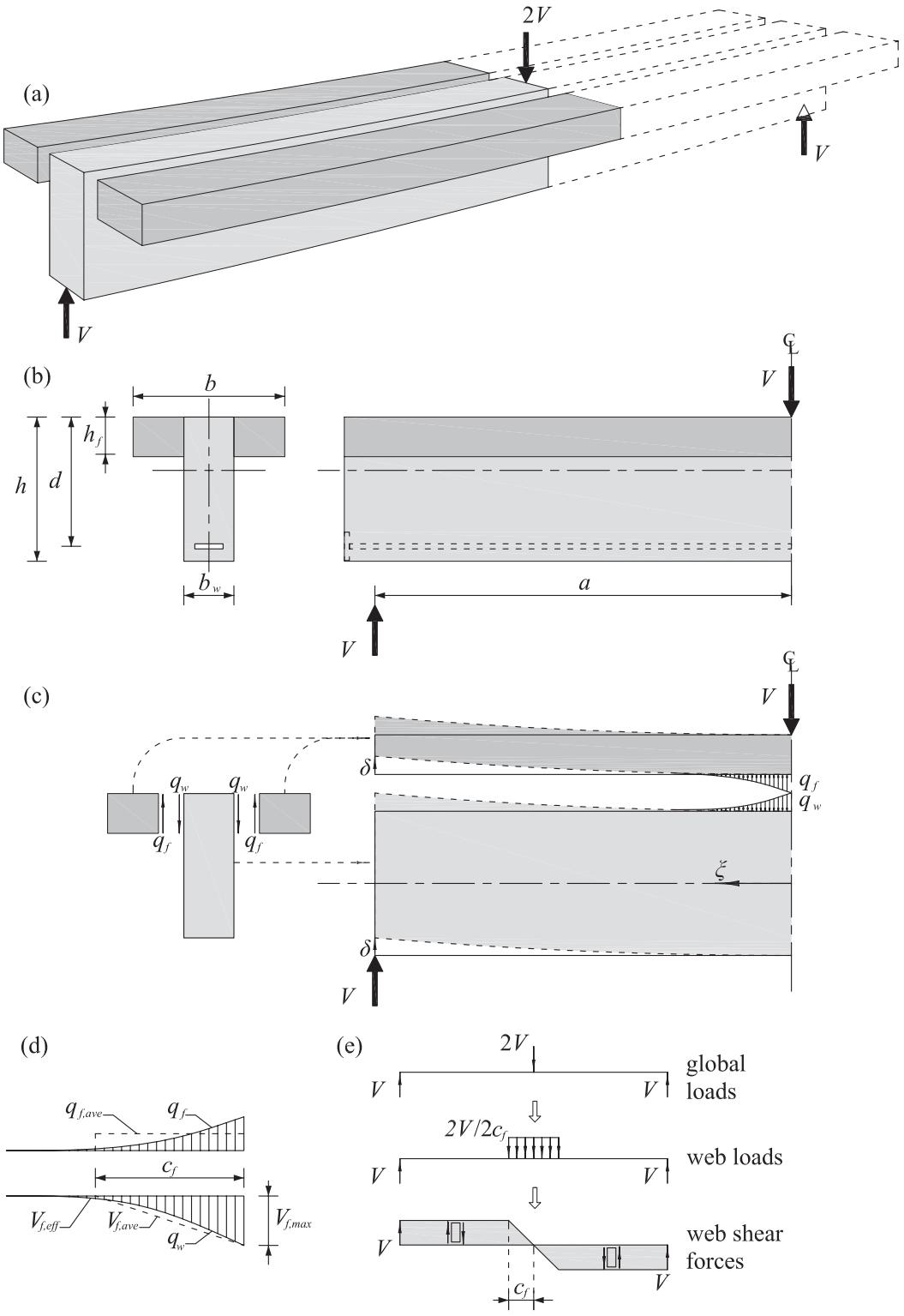

FIGURE 9 Flange–web interaction: (a) complete T-beam system, (b) dimensions, (c) flange–web interaction, (d) average loads and shear forces interaction, and (e) shifting of the control section.

prestressed girders with flanges as well as by numerical analyses with finite elements). Therefore, the second term of Equation 4 ($EI_w \cdot \partial^4\delta/\partial\xi^4$) is neglected. The use of this assumption based on the numerical work performed by Ruft et al[30] was in agreement with the test measurements of seven specimens with compressed flanges for the steps close to the failure.

As the equilibrium of forces must be satisfied for each section ($q_w = q_f$), by using these Equations 3 and 4:

$$EI_f \cdot \frac{\partial^4 \delta}{\partial \xi^4} = GA_w \cdot \frac{\partial^2 \delta}{\partial \xi^2} \tag{5}$$

The deflection δ can consequently be obtained from the solution of the differential Equation 5:

$$\delta = c_1 + c_2 \cdot \xi + c_3 \cdot \cosh(\lambda \cdot \xi) + c_4 \cdot \sinh(\lambda \cdot \xi) \quad (6)$$

with four constants (c_1–c_4) and a factor λ defined as:

$$\lambda = \sqrt{\frac{GA_w}{EI_f}} \quad (7)$$

The four constants in Equation 6 can be obtained by considering four boundary conditions along the shear span a. According to Figure 9b,c, the following boundary conditions are assumed:

- No deflection at $\xi = 0$: $\delta(0) = 0$.
- No rotation at $\xi = 0$: $\delta'(0) = 0$.
- No curvature at $\xi = a$: $\delta''(a) = 0$.
- Vertical equilibrium at $\xi = a$: $EI_f \cdot \delta'''(0) + GA_w \cdot \delta'(0) - V = 0$.

where V is the shear force imposed.

By introducing the boundary conditions into Equation 6, the deflection can be calculated as:

$$\delta = \frac{V}{GA_w} \cdot \left[B \cdot (1 - \cosh(\lambda \cdot \xi)) + \frac{1}{\lambda} \cdot \sinh(\lambda \cdot \xi) - \xi \right] \quad (8)$$

where

$$B = \frac{\sinh(\lambda \cdot a)}{\lambda \cdot \cosh(\lambda \cdot a)} = \frac{1}{\lambda} \tanh(\lambda \cdot a) \quad (9)$$

The distributed vertical load q_f that is transferred from the flange into the web (see Figure 9c) is based on Equation 6 of the deflection δ and can be calculated as:

$$q_f = EI_f \cdot \frac{\partial^4 \delta}{\partial \xi^4} = V \cdot \lambda \cdot [-B \cdot \lambda \cdot \cosh(\lambda \cdot \xi) + \sinh(\lambda \cdot \xi)] \quad (10)$$

And the shear force at the flange V_f can thus be calculated as:

$$V_f = EI_f \cdot \frac{\partial^3 \delta}{\partial \xi^3} = V \cdot [-B \cdot \lambda \cdot \sinh(\lambda \cdot \xi) + \cosh(\lambda \cdot \xi)] \quad (11)$$

Figure 9d shows the resulting vertical load q_f transferred between the flange and the web as well as the shear force in the flange V_f associated with this load. Although the load q_f takes a variable value along ξ, it can be assumed, in order to simplify the flange–web interaction, that the load transmitted between the flange and web is constant $q_{f,ave}$ along the length c_f.[30] This constant load results in a linear for the law shear force $V_{f,ave}$, as shown in Figure 9d. Assuming, according to Ruft et al,[30] it occurs that the average load $q_{f,ave}$ is half of the maximum value of the variable load q_f (that takes place at $\xi = 0$), the value of the load $q_{f,ave}$ can be calculated as:

$$q_{f,ave} = -0.5 \cdot q_f(0) = -0.5 \cdot V \cdot \lambda^2 \cdot B \quad (12)$$

Due to the fact that at $\xi = 0$, the shear force of the flange is maximum ($V_{f,max}$, see Figure 9d), and in order to ensure that the area of $q_{f,ave}$ is equal to the area of q_f, the length c_f can be calculated as:

$$c_f = -\frac{V_{f,max}}{q_{f,ave}} = \frac{-V}{q_{f,ave}} = \frac{2}{\lambda^2 \cdot B} \quad (13)$$

Note that the length c_f, assumed by simplifying a constant contact force between the flange and the web, is shorter than the actual one. This fact will lead to conservative results on the role of the flange as it will be shown later. For common values of the product $\lambda \cdot a$, B approaches $1/\lambda$. Therefore, by substituting $B = 1/\lambda$ in Equation 13, c_f can be calculated as:

$$c_f \cong \frac{2}{\lambda} = 2 \cdot \sqrt{\frac{EI_f}{GA_w}} \quad (14)$$

With respect to the parameters of Equation 14, the bending stiffness of the flange can be calculated as (uncracked flange according to Figure 6d):

$$EI_f = E_c \cdot \frac{(b - b_w) \cdot h_f^3}{12} \quad (15)$$

whereas the shear stiffness of the web can be expressed as:

$$GA_w = k_w \cdot \frac{E_c}{1 + \nu} \cdot b_w \cdot h \quad (16)$$

where E_c is the modulus of elasticity of concrete, ν is the Poisson's ratio, b and b_w refer to the widths of the flange and the web, respectively, and h_f and h refer to the flange depth and the total depth, respectively (see Figure 9b). The parameter k_w refers to the loss of stiffness due to web cracking This term is usually referred to as the "shear retention factor" in the literature. Values for this factor may vary depending on the structural problem (slabs subjected to torsion and bending, panels subjected to in-plane forces) and degree of cracking. In this work, the approach presented in References 31 and 32 will be followed due to its applicability to the problem and consistency with the assumptions of Rupf et al.[30] Thus, in the following, a constant value $k_w = 1/12$ will be adopted.[31]

Substituting Equations 15 and 16 into Equation 13, and assuming $d = 0.9 \cdot h$, one can obtain:

$$c_f \cong 3 h_f \sqrt{\frac{(b - b_w) \cdot h_f}{d \cdot b_w}} \quad (17)$$

As a result from the web–flange interaction, the section with maximum shear force is shifted by a length c_f toward the support (Figure 9e). Consequently, the linear increase on the shear force inside the distributed load region is faster than the parabolic decrease of the bending moment, and the section outside the load region is thus governing. Therefore, the control section of the CSCT (Figure 8a) should also be shifted by the same length. In the following, the control section in the CSCT for T-beams will be located at a distance $d/2 + c_f$ of the point load. It can be noted that

in case b is equal to b_w (rectangular beams), c_f will be equal to 0. Thus, a rectangular beam will be only a particular case, and the transition between T-beams and rectangular beams is smooth. The simplicity of use of the CSCT is thus retained, and the only modification of the analysis is the shift of the control section by a distance c_f.

For usual shapes of T-beams, the range of the ratio c_f/d is between 0 and 1.8. The ratio c_f/d for the dimensions of the test campaign conducted by Swamy et al,[17] whose results are shown in Figure 7 is, for instance, 0.88. It can be noted that if this value of c_f is plotted in Figure 7, it agrees well with the shift of the intersection vertex of Kani's valley between rectangular beams and T-beams. This is logical as the clear shear span of the web is reduced by the distributed load acting in the web as previously explained (Figure 9e).

These conclusions are also supported if the load-carrying actions are investigated by means of equilibrium-based models. As Figure 10 shows, the inclination of the strut carrying shear to the support is different when a point load or a distributed load is applied.

The angle of the strut corresponding to a point load (β_R, related to the beams with rectangular cross section) is:

$$\tan \beta_R = \frac{z}{a} \tag{18}$$

whereas the angle of the strut for a distributed load (β_T, related to the T-beams) satisfies the following relationship:

$$\tan \beta_T = \frac{z}{\left(a - \frac{c_f}{2}\right)} \tag{19}$$

Therefore, the strut associated with a distributed load is always steeper than that associated with a concentrated load. Consequently, beams loaded with a distributed load exhibit a behavior similar to that of beams with concentrated loads and shorter shear spans.[33]

4 | EXPERIMENTAL VERIFICATION

This section presents a comparison of different shear design models and the proposal based on the CSCT previously introduced with available test data on T-beams without transverse reinforcement. Other than the CSCT, the following shear design models have been used: Model Code 2010,[14] Eurocode 2,[34] and ACI-318,[35] as well as the model developed by Mari et al[36] and its extension for T-beams.[8] With respect to the tests, the following data have been collected from the literature (reinforced concrete beams with T-section without shear reinforcement): 24 beams reported by Ferguson and Thompson,[19] 25 beams by Al-Alusi,[20] 7 beams by Placas et al,[5] 178 beams by Kani et al,[28] 1 beam by Taylor and El-Hammasi,[37] and 4 beams by Palaskas et al.[38] Therefore, 239 beams of the abovementioned campaigns have been collected. From these specimens, only 147 elements have been selected for analysis following the selection criteria given below:

- The beams present a compression flange.
- The beams have a shear failure reported or have not reached the 99% of the theoretical bending plastic moment (in order to avoid shear failures after yielding of the flexural reinforcement).[39]
- The beams that have a shear span of $a \leq 2.5d + c_f$ have been removed in order to evaluate only slender members (refer to Figure 7).

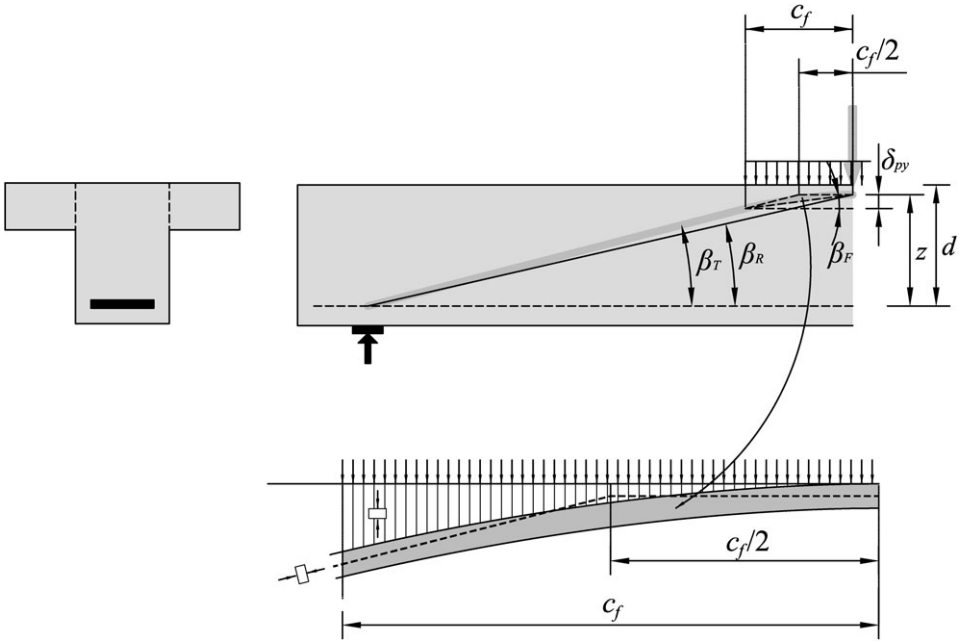

FIGURE 10 Geometrical comparison between a direct strut developing for a point load and a linear–parabolic strut developing for a distributed load over a distance c_f.

TABLE 1 Comparison of different procedures for T-beams without stirrups

Reference (year)	No.	V_{test}/V_{calc}	EC-2	ACI 318-11	MC10 Lev. II	Mari et al	Critical Shear Crack Theory
Ferguson and Thopson (1953)[19]	24	Average	1.10	1.66	1.12	0.99	1.02
		COV (%)	15.52	15.39	14.37	17.05	14.21
Al-Alusi (1957)[20]	13	Average	1.11	1.69	1.29	1.11	1.11
		COV (%)	8.62	8.19	6.78	11.45	6.34
Placas et al (1971)[5]	2	Average	1.31	1.80	1.34	1.22	1.18
		COV (%)	17.98	26.19	6.03	0.13	11.69
Kani et al (1979)[28]	104	Average	1.32	1.87	1.35	0.95	1.19
		COV (%)	21.42	21.63	10.15	13.01	12.40
Palaskas et al (1981)[38]	4	Average	1.05	0.94	1.24	1.06	1.11
		COV (%)	15.23	8.60	16.49	14.97	16.22
		Average	1.26	1.80	1.31	0.98	1.16
		COV (%)	21.41	22.14	12.44	14.48	13.46
		Median	1.191	1.700	1.311	0.954	1.155
		Standard deviation	0.269	0.398	0.162	0.142	0.156
		Minimum	0.85	0.86	0.92	0.71	0.81
		1% fractile	0.88	0.92	0.94	0.75	0.87
		5% fractile	0.94	1.28	1.04	0.78	0.92
		95% fractile	1.83	2.61	1.54	1.26	1.43
		99% fractile	2.09	2.92	1.72	1.33	1.61
		Maximum	2.20	3.05	1.76	1.36	1.66
Demerit point analysis							
Range	**Demerit points**	**Classification**					
<0.5	10	Extremely dangerous	0	0	0	0	0
0.5–0.67	5	Dangerous	0	0	0	0	0
0.67–0.85	2	Low safety	1	0	0	25	1
0.85–1.30	0	Appropriate safety	97	9	66	117	120
1.30–2.0	1	Conservative	46	97	81	5	26
>2.0	2	Extremely conservative	3	41	0	0	0
Total demerit points			54	179	81	55	28

Table 1 and Figure 11 show the comparison of measured-to-predicted shear strengths V_{test}/V_{calc} for the different design models. Table 1 provides the average, median, standard deviation, coefficient of variation, minimum, 1% percentile, 5% percentile, 95% percentile, 99% percentile, and maximum value of the ratios V_{test}/V_{calc}. In addition, the bottom of the Table 1 shows the demerit point evaluation according to Collins.[40]

The proposed model based on the CSCT gives fairly accurate predictions, with a very low value of coefficient of variation (13.2%). It can be noted that this value is similar to that of the CSCT for rectangular beams,[16] which implies that the modifications introduced are consistent with the original formulation and do not introduce additional scatter. The CSCT predicts the shear strength better than the other proposals. In addition, the demerit point analysis[40] ranks the proposal as the best for shear design purposes, followed by the Eurocode 2, the Mari et al's model, the Model Code 2010, and the ACI-318.

The correlation between the shear strength observed at tests and the shear strength predicted for the 147 beams is compared in Figure 11 to the different models in terms of the ratios: a/d, h_f/d, and $\rho_l = A_s/(b_w \cdot d)$. It can be observed that the Eurocode 2 and the ACI predictions have a large scatter of ratios of a/d lower than 4 and of ratios h_f/d higher than 0.37. The reason for these disagreements is related to the fact that these shear design procedures do not account explicitly for the role of the flanges (leading to safer predictions for larger longitudinal reinforcement ratios or flanges).

However, the predictions made by the Model Code 2010, by Mari et al's model, and by the CSCT proposal do not clearly show these trends as they account for the role of the flanges.

5 | CONCLUSIONS

The present paper investigates the behavior and strength of T-beams without shear reinforcement. Its main conclusions are:

1. Through the analysis of cracking patterns and kinematics at failure, it is justified that the STA of T-beams are

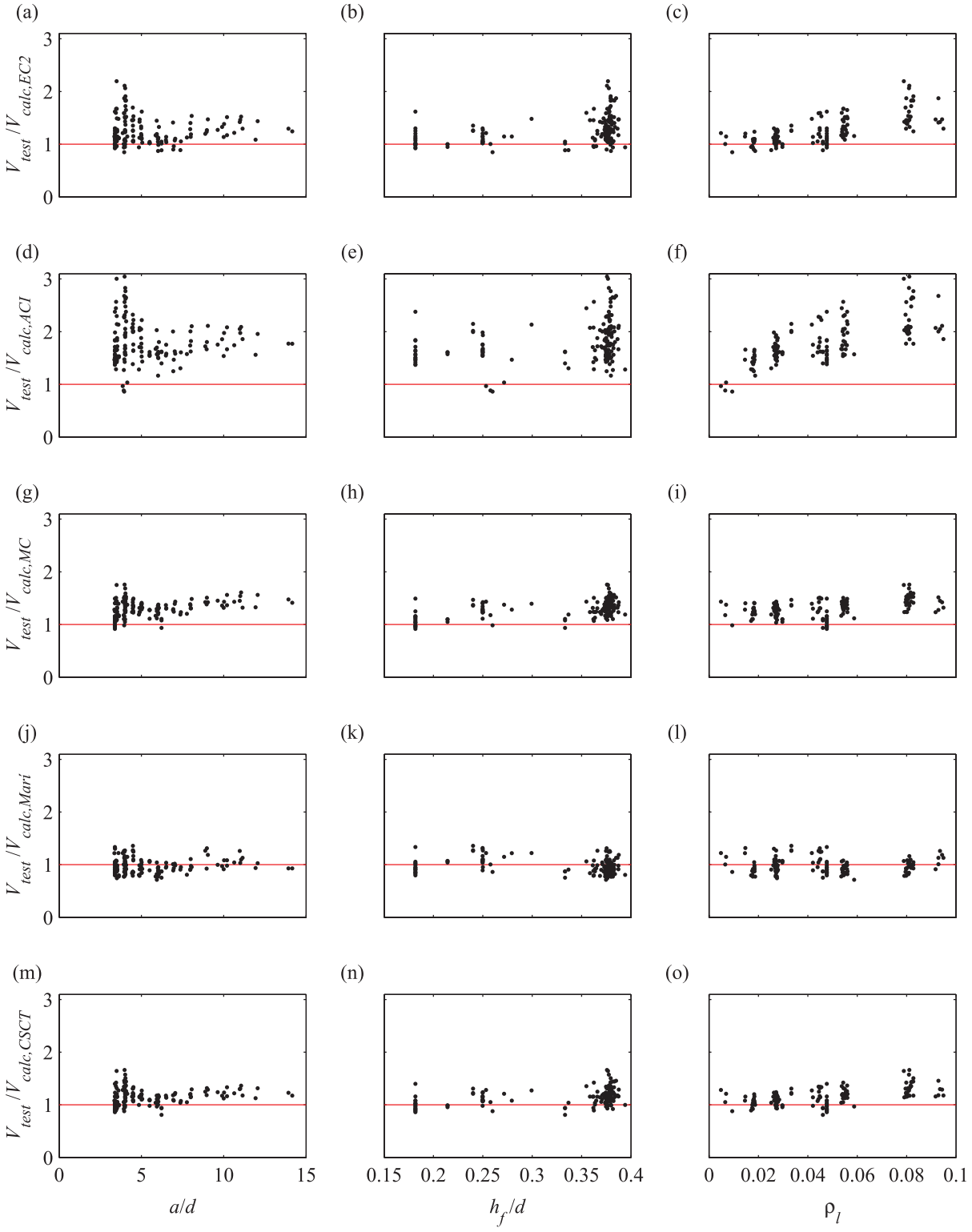

FIGURE 11 Correlation between the shear strength observed at tests V_{test} and the shear strength-predicted V_{calc} for the 147 beams in terms of the ratios: a/d, h_f/d, and $\rho_l = A_s/(b_w \cdot d)$ for (a–c) ACI, (d–f) Eurocode 2, (g–i) Model Code 10, (j–l) Marí model, and (m, n) Critical Shear Crack Theory proposal.

different to those of beams with a rectangular cross section.

2. A rational analysis of the flange–web interaction is presented based on the relationships of its stiffness. This approach considers the flange an element that is smearing the applied loads in the web over a given length.
3. On that basis, a rational explanation of the shift of the bottom of Kani's valley between rectangular cross section beams and T-beams (from $a/d = 2.5$ toward $a/d = 4$) is provided.
4. Based on previous points, an extension of the CSCT has been proposed in order to assess the shear strength of T-beams without shear reinforcement, in which the

beams with a rectangular cross section remain a particular case.

5. The proposal has been checked with experimental results available in the literature and compared with the Model Code 2010, Eurocode 2, ACI-318, and the shear model of Mari et al. The results of this comparison show the CSCT to be the most suitable shear design model for T-beams, without shear reinforcement accounting for its demerit points
6. The proposed extension of the CSCT is simple enough to be used for practical purposes as only a shift of the location of the control section is required.

NOTATIONS

a	shear spam
A_w	area of the web
b	maximum width of the section
b_w	web width
c_f	length of flange–web load interaction
d	effective depth
d_g	maximum aggregate size
d_{g0}	reference aggregate size
E_c	concrete modulus of elasticity
f_c	cylinder concrete compressive strength
G	concrete shear modulus
h	total depth
h_f	flange depth
I_f	inertia of the flange
I_w	inertia of the web
k_i	coefficients related to loss of stiffness
q_f	flange distributed load
$q_{f,ave}$	average load applied to the flange
q_w	web distributed load
V	acting shear force
V_{calc}	calculated shear strength
V_f	shear forces applied to the flange
V_R	shear strength
V_{test}	observed shear strength at test
w	crack width
z	lever arm
β_F	average angle of a strut in a parabola
β_R	angle of a strut in a rectangular beam
β_T	angle of a strut in a T-beam
δ	deflection
δ_{py}	vertical distance of a parabola
ε	reference longitudinal strain
ξ	longitudinal axis
ν	Poisson's ratio

ACKNOWLEDGMENTS

The present work has been developed under the framework of research projects AGB-2006-015 and BIA2015-64672-C4-3-R (Horvital), funded by the Swiss Confederation and by the Spanish Ministry of Economics and the European Funds for Regional Development, respectively.

REFERENCES

1. Morsch E. *Concrete-Steel Construction (Der Eisenbetonbau)*. English translation of the 3rd German edition; 1909.
2. Somes NF, Corley WG. Circular openings in webs of continuous beams. *Am Concr Inst SP*. 1974;42:359-397.
3. Lau TL, Clark LA. Shear transfer between ribbed slab and internal column. *Mag Concr Res*. 2007;59:507-516.
4. Ribas C, Cladera A. Experimental study on shear strength of beam-and-block floors. *Eng Struct*. 2013;57:428-442.
5. Placas A, Regan PE, Baker ALL. Shear failure of reinforced concrete beams. *ACI J*. 1971;68:763-773.
6. ACI/ASCE Task Committee 426. The shear strength of reinforced concrete members. *ACI J*. 1973;99:1091-1187.
7. Leonhardt F. Shear and torsion in prestressed concrete. In: VI Fip Congress Prague, Session IV, 1970:48.
8. Cladera A, Marí A, Ribas C, Bairán J, Oller E. Predicting the shear-flexural strength of slender reinforced concrete T and I shaped beams. *Eng Struct*. 2015;101:386-396.
9. Moayer M, Regan PE. Shear strenght of prestressed and reinforced concrete T-beams. *Am Concr Inst SP*. 1974;42:183-213.
10. Swamy RN, Qureshi SA. An ultimate shear strength theory for reinforced concrete T-beams without web reinforcement. *Matériaux Constr*. 1974;7:181-189.
11. Zararis IP, Karaveziroglou MK, Zararis PD. Shear strength of reinforced concrete T-beams. *ACI Struct J*. 2006;103:693-700.
12. Tureyen AK, Wolf TS, Frosch RJ. Shear strength of reinforced concrete T-beams without transverse reinforcement. *ACI Struct J*. 2006;103:656-663.
13. Ribas C, Cladera A, Mas B. Modelo cortante-flexión para el dimensionamiento a ELU de forjados de vigueta pretensada y bovedilla. In: VI Congreso Internacional de Estructuras ACHE, 2014:151–152; Madrid, Spain.
14. *fib*: Model Code 2010. Fédération Internationale du Béton, 2010.
15. Fernández M, Muttoni A, Sagaseta J. Shear strength of concrete members without transverse reinforcement: a mechanical approach to consistently account for size and strain effects. *Eng Struct*. 2015;99:360-372.
16. Muttoni A, Fernandez M. Shear strength of members without transverse reinforcement as function of critical shear crack width. *ACI Struct J*. 2008;105:163-172.
17. Swamy RN, Andriopoulos A, Adepegba D. Arch action and bond in concrete shear failures. *J Struct Div*. 1970;96:1069-1091.
18. Placas A. *Shear Failure of Reinforced Concrete Beams*. PHD thesis. FacultyEngineering of the University of London. Imperial College of Science and Technology, London.; 1969.
19. Ferguson PM, Thompson JN. Diagonal tension in T-beams without stirrups. *ACI J Proc*. 1953;49:665-675.
20. Al-Alusi AF. Diagonal tension strength of reinforced concrete T-beams with varying shear span. *ACI J*. 1957;53:1067-1077.
21. Kotsovos MD, Bobrowski J, Eibl J. Behaviour of reinforced concreteT-beams in shear. *Struct Eng Part B R&D Q*. 1987;65(B):1-10.
22. Regan PE. *Comments on the Model Code Clauses for Shear and Torsion*. Polytechnic of Central London, London; 1978.
23. Kotsovos MD, Bobrowski J, Eibl J. Behaviour of reinforced concreteT-beams in shear. *Struct Eng*. 1987;65B:1-10.
24. Park H-G, Kang S, Choi K-K. Analytical model for shear strength of ordinary and prestressed concrete beams. *Eng Struct*. 2013;46:94-103.
25. Muttoni A, Schwartz J. Behaviour of beams and punching in slabs without shear reinforcement. In: IABSE Colloquium, 1991, 703–708; Zurich, Switzerland.
26. Zararis PD, Papadakis GC. Diagonal shear failure and size effect in RC beams without web reinforcement. *J Struct Eng*. 2001;127:733-742.

27. Collins MP, Mitchell D. *Prestressed Concrete Structures*. Englewood Cliffs, NJ: Prentice Hall; 1991.

28. Kani MW, Huggins MW, Wittkopp RR. *Kani on Shear in Reinforced Concrete*. Dept. of Civil Engineering, University of Toronto, Canada; 1979.

29. Bazant ZP, Gambarova P. Rough cracks in reinforced concrete. *J Struct Div*. 1980;106:819-842.

30. Rupf M, Fernández Ruiz M, Muttoni A. Shear strength of prestressed bridges with insufficient shear reinforcement (in German: Querkraftwiderstand vorgespannter Brücken mit ungenügender Querkraftbewehrung). Rapport 658, Département fédéral des transports, des communications et de l'énergie, Office fédéral des routes, Bern, Switzerland, 2014:88.

31. Nielsen MP, Hoang LC. *Limit Analysis and Concrete Plasticity*. 3rd ed. Boca Raton, FL: Taylor & Francis Group; 2011.

32. Crisfield MA, Wills J. Analysis of R/C panels using different concrete models. *J Eng Mech*. 1989;115:578-597.

33. Pérez Caldentey A, Padilla P, Muttoni A, Fernández Ruiz M. Effect of load distribution and variable depth on shear resistance of slender beams without stirrups. *ACI Struct J*. 2012;109:595-603.

34. Eurocode 2. *Design of Concrete Structures. Part 1: General Rules and Rules for Buildings, European Committee for Standarization*. Brussels, Belgium: CEN; 2002.

35. ACI Committee 318. *Building Code Requirements of Structural Concrete and Commentary*. ACI. American Concrete Institute 38800 Country Club Drive Farmington Hills, MI 48331 U.S.A.; 2011.

36. Marí AR, Cladera A, Bairán J, Oller E, Ribas C. Shear-flexural strength mechanical model for the design and assessment of reinforced concrete beams subjected to point or distributed loads. *Front Struct Civ Eng*. 2014;8:337-353.

37. Taylor MA, El-Hammasi S. Web cracking behavior of beams using welded wire fabric as shear reinforcement. *ACI J Proc*. 1980;77:12-17.

38. Palaskas MN, Attiogbe EK, Darwin D. Shear strength of lightly reinforced T-beams. *J Am Concr Inst*. 1981;78:447-455.

39. Vaz Rodrigues R, Muttoni A, Fernández Ruiz M. Influence of shear on rotation capacity of reinforced concrete members without shear reinforcement. *ACI Struct J*. 2010;107(5):516-525.

40. Collins MP. Evaluation of shear design procedures for concrete structures. A report prepared for the CSA Technical Committee on Reinforced Concrete Design, Canada, March 2001.

AUTHOR'S BIOGRAPHIES

Carlos R. Ribas González is a lecturer at the Department of Physics at the Universitat de les Illes Balears, Spain. His research focuses on: Mechanical models for the behaviour of concrete members and structures; application of shape memory alloys in structural engineering and precast concrete structures.

FIB member, Miguel Fernández Ruiz is Senior Lecturer and Scientist at the School of Architecture, Civil, and Environmental Engineering (ENAC) of École Polytechnique Fédérale de Lausanne (EPFL), Switzerland. His research interests include the serviceability behaviour of structures, bond, shear and punching shear, and the modelling of structural concrete using stress fields.

How to cite this article: Ribas González CR and Fernández Ruiz M. Influence of flanges on the shear-carrying capacity of reinforced concrete beams without web reinforcement. *Structural Concrete.* 2017;18:720–732. https://doi.org/10.1002/suco.201600172